ROYAL SOCIETY
OF CHEMISTRY

PAPER

Check for updates

Switching between DNA binding modes with a photo- and redox-active DNA-targeting ligand, part II: the influence of the substitution pattern†

Christoph Dohmen and Heiko Ihmels ⓘ *

A disulfide-functionalized photoactive DNA ligand is presented that enables the control of its DNA-binding properties by a combination of a photocycloaddition reaction and the redox reactivity of the sulfide/disulfide functionalities. In particular, the initially applied ligand binds to DNA by a combination of intercalation and groove-binding of separate benzo[*b*]quinolizinium units. The association to DNA is interrupted by an intramolecular [4 + 4] photocycloaddition to the non-binding head-to-head cyclomers. In turn, the subsequent cleavage of these cyclomers with dithiothreitol (DTT) regains temporarily a DNA-intercalating benzoquinolizinium ligand that is eventually converted into a non-binding benzothiophene. As a special feature, this sequence of controlled deactivation, recovery and internal shut-off of DNA-binding properties can be performed directly in the presence of DNA.

Introduction

DNA-binding ligands continue to be an essential and indispensable basis for the development of DNA-targeting agents, especially as chemotherapeutic drugs in cancer therapy.[1] However, most DNA-targeting drugs also induce damage in healthy cells, which leads to severe side effects in chemotherapy. Therefore, there is still a great need for novel drugs with high selectivity towards the target cell and DNA.[2,3] To increase the drug selectivity, prodrugs have been developed,[2,4] namely inactive or inert substances which can be transformed into their desired bioactive form by an external chemical or physical stimulus.[5,6] Along these lines, the application of reductive cleavage of disulfides to activate the prodrug has been established as promising approach because some tumor cells have low oxygen levels and contain higher amounts of L-glutathione (GSH),[5,7,8] which in turn reduces the inactive disulfides to their corresponding bioactive thiols.[5,9,10] In addition, the disulfide functionality provides an additional favorable property because it may increase drug permeability, specifically through cell membranes.[10,11] Alternatively, photoactive DNA-targeting drugs may be activated or deactivated by

light.[12] This approach offers the advantage that the photoinduced ligand generation can be applied with high temporal and local control, and that it does not depend on diffusion-controlled processes in the case of unimolecular and/or intramolecular photoreactions.[13] Hence, several efficient photochromic systems have been investigated, whose DNA-binding properties can be switched even reversibly by light.[12] With these tools in hand, it seems to be particularly attractive to be able to activate or deactivate a ligand by several stimuli simultaneously or complementarily in order to ensure a larger range of application and also the variable adaptation to the medium. However, only one example of a combination of a sulfide-mediated redox process and a photochemical conversion for the control of DNA-binding properties of a ligand has been reported, so far.[14] In the latter study, the redox-active disulfide functionality has been combined with the photochromic DNA-binding benzo[*b*]quinolizinium ion (**1**), which provides the complementary photochemical control element.[15–19] In particular, the 9-dialkyldisulfide-linked bis-benzo[*b*]quinolizinium derivative **4a** can either be reduced to the thiol **3a** or transformed into its cycloadducts **c4a**[shh] and **c4a**[sht] by an intramolecular photocycloaddition reaction. This sequence allows the controlled formation of ligand–DNA complexes with different binding modes depending on the stimulus (Fig. 1),[14] which provides a proof of concept for a dual-mode controllable DNA-targeting system. But the employed model compound **4a** still requires further optimization because the intramolecular photoreaction results in a mixture of three products and the binding affinities of the ligands are relatively low, as compared

Department of Chemistry – Biology, University of Siegen, and Center of Micro- and Nanochemistry and (Bio)Technology (Cμ), Adolf-Reichwein-Str. 2, 57068 Siegen, Germany. E-mail: ihmels@chemie.uni-siegen.de

†Electronic supplementary information (ESI) available: Materials, methods, experimental procedures, analytical data and spectra. See DOI: https://doi.org/10.1039/d3ob00879g
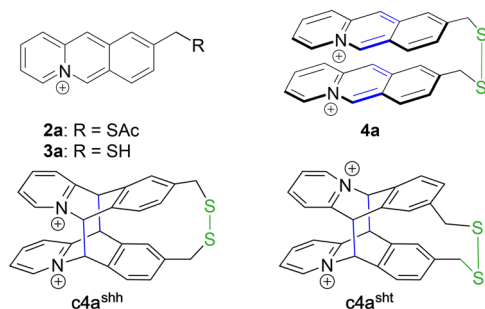
This journal is © The Royal Society of Chemistry 2023

Org. Biomol. Chem., 2023, **21**, 5799–5808 | 5799

Fig. 1 Photo- (blue) and redox- (green) active benzo[*b*]quinolizinium derivative **4a** and products **c4a**^{shh} and **c4a**^{sht} from the intramolecular photocycloaddition of **4a**.

with the ones of other quinolizinium based DNA binders.[15,16,18] Therefore, structural variations are required that lead to a more selective photoreaction and an increased affinity of the DNA-binding elements of the photochromic equilibrium. A possible starting point for such studies may focus on the position of the linking dialkyldisulfide, because it is well known that the position of the linker unit in bis-anthracenes has a strong influence on the course of the intramolecular photocycloaddition,[20] and that the substitution pattern of quinolizinium derivatives leads to different DNA-binding properties.[16] With this object, it may be proposed that the relocation of the linker unit in **4a** from position C9 to C7 of the benzo[*b*]quinolizinium unit, as realized in the isomeric disulfide **4b** (Scheme 1), should lead to significantly different photochemical and DNA-binding properties. Herein, we will report on the synthesis and investigation of the disulfide **4b** and show that, indeed, it may also serve as platform for dual-mode addressable DNA ligands; however, with very different photochemical and DNA-binding parameters as well as chemical reactivity, as compared with the ones of **4a**.

Results and discussion

Synthesis

The nucleophilic substitution of 7-bromomethyl-benzo[*b*]quinolizinium bromide[21] (**5**) with thioacetic acid furnished the thioacetate **2b** in 83% yield (*cf.* Experimental section). Acid-catalyzed thioester cleavage gave the intermediate thiol **3b**, which was subsequently oxidized with bromine to the disulfide **4b** in a 91% yield over two steps (Scheme 1). The thioacetate **2b** and the disulfide **4b** were fully characterized and identified by 1D- and 2D-NMR spectroscopy, absorption and emission spectroscopy, and elemental analysis (*cf.* Experimental section, *cf.* ESI, chapter 6†).

The ^{1}H-NMR-spectroscopic analysis of the reaction mixture from the thioester cleavage of **2b** under anaerobic conditions pointed to the presence of the respective thiol **3b** as major product of the reaction, as indicated by the characteristic shifts and multiplicities of the protons from the CH$_2$SH group (CH$_2$: 4.44 ppm, d, 8 Hz; SH: 3.55 ppm, t, 8 Hz; *cf.* ESI, Fig. S43†). However, in contrast to the thiol **3a**, which quickly oxidizes to the corresponding disulfide **4a**, the thiol **3b** was converted into another product. Namely, after 5 h the ^{1}H-NMR spectrum indicated the presence of a product without the characteristic signal of the 6-H proton (**3b**, s, 10.70 ppm) of the benzo[*b*]quinolizinium (*cf.* ESI, Fig. S1†). Furthermore, the four aromatic proton signals at 7.78 ppm (d, 8 Hz, 1H), 7.82 ppm (t, 7 Hz, 1H), 8.35 ppm (t, 8 Hz, 1H), and 8.81–8.84 ppm (m, 1H) pointed to the presence of a pyridine ring, which is connected to another aromatic unit by a methylene group with a NMR shift of 4.64 ppm (s, 2H). The second aromatic unit has seven protons, and the signal at 8.08 ppm (s, 2H) is consistent with the respective 1-H and 3-H proton signals of benzo-annelated thiophenes, which typically appear at 7.51–7.97 ppm.[22] Based on these ^{1}H-NMR-spectroscopic data, and in combination with the consistent 2D-NMR-spectroscopic data and a correct exact mass (*cf.* ESI, Fig. S3–7†), the
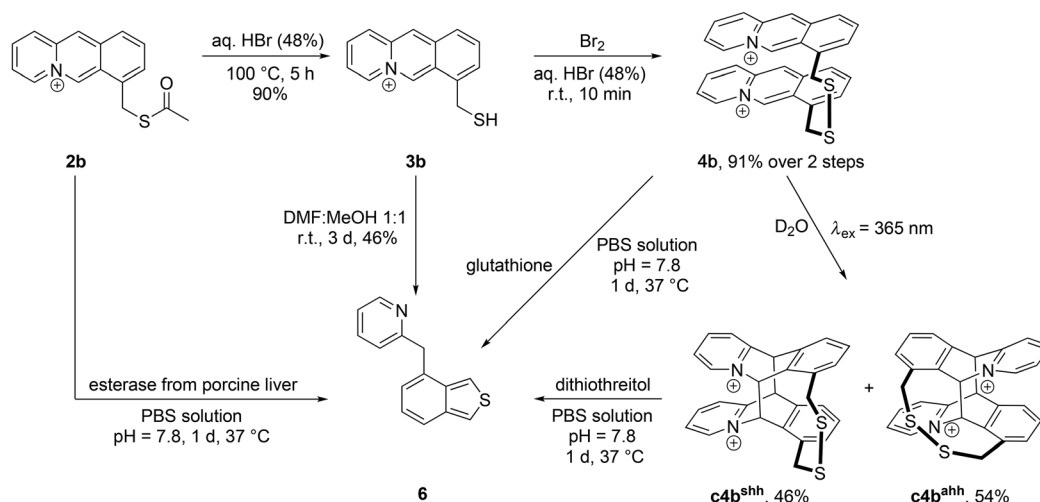
Scheme 1 Synthesis of bis(benzo[*b*]quinolizinium)disulfide **4b** and benzo[*c*]thiophene derivative **6** (counter ion Br⁻ omitted for clarity).

5800 | *Org. Biomol. Chem.*, 2023, **21**, 5799–5808

This journal is © The Royal Society of Chemistry 2023

structure was assigned to the so far unknown 2-(benzo[c]thio-phen-4-ylmethyl)pyridine (**6**).

Mechanistic studies on the formation of 6

The conversion of the thiol **3b** to the benzo[c]thiophene **6** was further investigated by ¹H-NMR spectroscopy. In a CD₃OD solution, the spectrum recorded directly after sample preparation showed exclusively the proton signals of the thiol **3b** (*cf.* ESI, Fig. S15†), as indicated by the characteristic shift and multiplicity of the methylene protons (see above, *cf.* ESI, Fig. S43†). After 5 d at room temperature, the ¹H-NMR spectrum revealed a mixture of mainly the thiol **3b** (11%) and the product **6** (85%). The methylene group of the latter was deuterated as the integration of the NMR signal corresponded to only one proton (*cf.* ESI, Fig. S16†). Moreover, the NMR-spectroscopic analysis indicated that the formation of **6** from **3b** proceeded through at least one intermediate as indicated by a third set of signals that appeared after 3 h and after 1 d, and that eventually disappeared after 5 d. Because of the signal overlap, it was not possible to determine meaningful structural details of this intermediate, except that it lacks the characteristic 6-H proton signal of a benzo[b]quinolizinium.

The conversion of **3b** was also monitored by NMR spectroscopy in D₂O solution. In this solvent, the ¹H-NMR spectrum recorded directly after sample preparation indicated a rapid formation of a product mixture that no longer contained the starting material. Instead, the main component of the reaction mixture showed a ¹H-NMR spectrum with two spin systems in the aromatic range, both of which contain four protons (*cf.* ESI, Fig. S9†). One spin system showed the characteristic pattern of a 2-substituted pyridine derivative (8.00 ppm, t, 7 Hz, 1H; 8.14 ppm, d, 8 Hz, 1H; 8.48 ppm t, 8 Hz, 1H; 9.21 ppm d, 7 Hz, 1H; *cf.* ESI, Fig. S9C†). In addition, signals of a methylene group at 4.81 ppm (d, 14 Hz) and of a neighboring aliphatic proton at 4.52 ppm (dd, 14 Hz, 3 Hz, 1H) were detected. The latter proton signal is in the same region as that of the 6-H proton signal in 6H-pyrido[1,2-b]isoquinoline derivatives,[23] and the CH proton signal in thioaminals.[24,25] With these spectroscopic data and additional 2D-NMR experiments the product was assigned to the 2,11a-dihydropyrido[1,2-b]thieno[4,3,2-ij]isoquinoline (**7**) (Scheme 2, *cf.* ESI, Fig. S9–13†). The reaction of intermediate **7** to the benzo[c]thiophene **6** was not observed even with longer reaction time. Instead, a precipitate formed slowly and a ¹H-NMR spectrum of the suspension after 2 d indicated that compound **7** decomposed steadily to a complex mixture of unidentified products (*cf.* ESI, Fig. S14†). In contrast, the transformation of **3b** into **6** took place in a dilute aqueous phosphate buffer solution, which was shown photometrically. Thus, within 1 d, the characteristic absorption of the benzo[b]quinolizinium chromophore at 320–440 nm decreased, and the absorption bands of **6** at 320–370 nm and 280–310 nm evolved (Fig. 3A). However, a broad absorption band between 370–440 nm was also detected that did not correspond to **6** as compared with the absorption of an authentic sample (Fig. 3A). This absorption may belong either to non-converted starting material or a byproduct of this reaction.
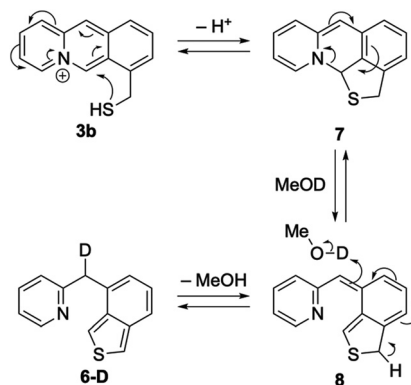
Scheme 2 Proposed mechanism for the formation of benzothiophene **6** from **3b**.

Considering the reactivity of the benzo[b]quinolizinium ion towards nucleophiles at the electrophilic C6-position,[18,26] the formation of the benzothiophene **6** is likewise introduced by an intramolecular nucleophilic addition of the thiol functionality to give, after deprotonation, the intermediate **7** (Scheme 2). In similar reactions, structurally related sulfanylalkyl-substituted phenanthridinium and isoquinolinium derivatives are converted to cyclic thioaminals.[24] In the case of **7**, an electrocyclic ring-opening reaction to the derivative **8** follows, as usually observed for addition products of benzoquinolizinium derivatives.[18,19,23,26,27] Eventually, a tautomerization leads to product **6**. This mechanism also explains the deuteration at the methylene group of **6** in the presence of MeOD (Scheme 2).

Photochemical properties

The absorption and emission properties of the thioacetate **2b** and the disulfide **4b** were investigated in different solvents (*cf.* ESI, chapter 2†). Thus, **2b** and **4b** exhibited the characteristic absorption bands of the benzo[b]quinolizinium chromophore with a long-wavelength absorption band with three maxima between 340–440 nm. The shifts of the absorption maxima are essentially independent of the solvent. The compounds **2b** and **4b** emit with broad bands in the range from 426 nm (**2b** in THF) to 464 nm (**4b** in CH₂Cl₂). The fluorescence intensity of **4b** is very low in all the investigated solvents ($\Phi_{Fl} < 0.01$), whereas the fluorescence quantum yields of **2b** are generally higher and increase with increasing polarity of the solvent, that is, from $\Phi_{Fl} < 0.01$ in EtOAc (**2b**) to $\Phi_{Fl} = 0.25$ (**2b**) in H₂O.

The photoreaction of the disulfide **4b** was monitored by absorption spectroscopy. When **4b** was irradiated with $\lambda_{ex} = 365$ nm the initial absorption bands of the benzoquolizinium chromophore steadily decreased, and an isosbestic point at 216 nm was formed (*cf.* ESI, Fig. S23A†). This observation indicated the [4 + 4] photodimerization of the benzoquinoliziniumunits,[19,28] in particular, as the resulting absorption spectrum resembled the ones of known photodimers.[19] The photoreaction took 11 min for completion, which is slower than the intramolecular photodimerization of the

This journal is © The Royal Society of Chemistry 2023

Org. Biomol. Chem., 2023, **21**, 5799–5808 | **5801**

isomer **4a** (2 min), but still substantially faster than the intermolecular photocycloaddition of the parent monomer,[14] so that it provided first evidence for an intramolecular photocycloaddition reaction of **4b**.

To gain more information about the structure of the photoproducts, the photoreaction of disulfide **4b** in a D_2O solution was monitored by ^{1}H-NMR spectroscopy. After 13 min of irradiation **4b** was converted into two main products (*ca.* 93%), as indicated by two independent sets of NMR signals (Fig. 2). Both products have the characteristic features of a head-to-head benzo[b]quinolizinium dimer, that is, two singlets of the bridgehead protons, respectively, in the region of 5–6 ppm (11-H) and 7–7.5 ppm (6-H). Additional analysis by 2D-NMR spectroscopy and mass spectrometry led to the assignment of the *syn*-head-to-head photocyclomer **c4**[shh] (46%) and the *anti*-head-to-head product **c4**[ahh] (54%) (*cf.* ESI, chapter 3.2†), in particular by comparison with the reported characteristic ^{1}H-NMR shifts of the doublets of the 4-H protons of the parent dimers of **1** (**1**[shh]: 9.38 ppm, **1**[ahh]: 9.19 ppm, **c4**[shh]: 9.21 ppm, **c4**[ahh]: 9.07 ppm).[14,17,19] Overall, these results showed that the disulfide-bridged quinolizinium **4b** reacts in a fast intramolecular photocycloaddition, like its isomer **4a**, however, with increased selectivity because the disturbing photoinduced disulfide cleavage does not take place in this case. Presumably, the photoinduced electron transfer (PET) reaction that is proposed to lead to disulfide cleavage in the photocyclomers of **4a**[29] is not energetically favorable in **c4b**[shh] and **c4b**[ahh].

The photoproducts turned out to be thermally stable at physiological conditions in solution, as indicated by negligible changes of their absorption spectrum at 37 °C for 16 h in aqueous buffer solution, even in the presence of DNA (*cf.* ESI, Fig. S24†). In contrast, when **c4b**[shh] and **c4b**[ahh] were irradiated for 5 min and 15 min with λ_{ex} = 310 nm the characteristic absorption band of the benzo[b]quinolizinium ion at 340–425 nm developed to 26% and 31% of the original absorbance of **4b**, respectively, indicating a photoinduced cycloreversion reaction that reached a photostationary state between **4b** and the cyclomers (*cf.* ESI, Fig. S23B†). Furthermore, this absorption band did not fully match the one of compound **4b** because during the irradiation an additional red-shifted

shoulder formed with zero-onset at *ca.* 580 nm. This observation indicated that there was at least one by-product formed along with the cycloaddition/cycloreversion products (*cf.* ESI, Fig. S23B†). Presumably, like in the case of isomer **4a** and its cycloadducts,[14] the disulfide bond was also cleaved at this excitation wavelength and the resulting thiyl radicals led to the formation of by-products.[30]

Reductive generation of 6

As disulfide **4a** and its photoproducts are reduced to the thiol **3a** by GSH or dithiothreitol (DTT),[14] the reactions of the corresponding isomer **4b** and its photocyclomers with GSH and DTT were also investigated. When the disulfide **4b** was treated with GSH under anaerobic conditions,[14] the absorption bands of the benzoquinolizinium steadily decreased, and the blue-shifted bands of the benzo[c]thiophene **6** evolved after 1 d (Fig. 3B). In addition, the same absorption band at 370–440 nm was detected as in the conversion of **3b** to **6** (see above). Likewise, the reduction of the photocyclomers **c4b**[shh] and **c4b**[ahh] with DTT resulted in the formation of product **6** as indicated by the same characteristic absorption spectrum after 1 d (Fig. 3C). However, the initial development and subsequent decrease of an absorption band with three maxima between 340–420 nm indicated the intermediate formation of a benzo[b]quinolizinium derivative, most likely the thiol **3b**. Furthermore, at the end of the reaction the absorption band at 370–440 nm was more intense than the one observed during the reduction with GSH, which indicated a higher concentration of the respective side product.
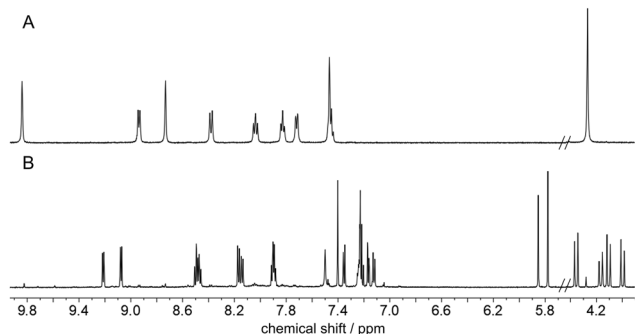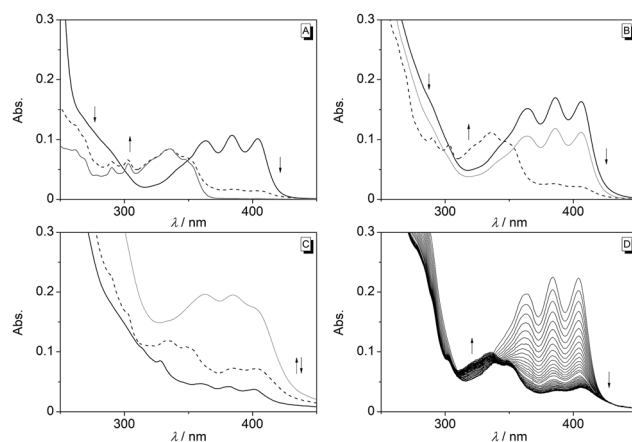

Fig. 3 A: Absorption spectra of **3b** (*c* = 20 μM, straight black line) and **6** (*c* = 20 μM, straight grey line) in phosphate buffered saline (PBS) solution (pH = 7.8) at 20 °C, and absorption spectrum of **3b** after 1 d at 37 °C (dashed line). B: Absorption spectra of **4b** (*c* = 10 μM) in PBS solution (pH = 7.8) at 20 °C (straight line) and after 1 d at 37 °C in the presence of GSH (*c* = 10 mM, dashed line). C: Absorption spectra of **c4b**[shh] and **c4b**[ahh] (*c* = 20 μM, derived from **4b**, *c* = 40 μM) in PBS solution (pH = 7.8) at 20 °C (straight line), after 4 h at 37 °C in the presence of DTT (*c* = 1 mM, grey line) and after 1 d (dashed line). D: Changes of absorption spectra during reaction of **2b** (*c* = 20 μM) with porcine liver esterase (400 μg, 7.6 units) in PBS solution (pH = 7.8) at 37 °C for 1 d.

Fig. 2 ^{1}H-NMR spectra (500 MHz) of the disulfide **4b** (A) and the photoproduct **c4b**[shh] and **c4b**[ahh] (B) after irradiation (λ_{ex} = 365 nm) of **4b** for *t* = 13 min in D_2O.

As the formation of the intermediate thiol **3b** is essential for the subsequent reaction to give the benzothiophene **6**, it was attempted to generate the intermediate **3b** independently by treatment of the thioacetate **2b** with esterase, specifically because this is a mild and biocompatible method. When the thioacetate **2b** was incubated with the esterase for 1 d at 37 °C the absorption bands of **2b** decreased, and the absorption spectrum of the benzo[*c*]derivative **6** evolved (Fig. 3D). However, the absorbance of the above-mentioned side product was also detected in this experiment.

Overall, these experiments demonstrated that the intermediate thiol **3b** is generated by the reduction of the disulfide **4b** or its photoproducts **c4b**[shh] and **c4b**[ahh] and complementary by the enzyme-catalyzed thioacetate cleavage of **2b**. And these reactions finally lead to the formation of the benzo[*c*]thiophene derivative **6**.

DNA-binding properties

The DNA-binding properties of the thioacetate **2b**, which was used as a suitable sulfur-functionalized reference compound, the disulfide **4b**, the photocyclomers **c4b**[shh] and **c4b**[ahh], and **6** with calf thymus (ct) DNA were investigated with photometric (Fig. 4, *cf.* ESI, chapter 5.1†) and fluorimetric titrations (*cf.* ESI, chapter 5.1 and 5.2†) in aqueous buffer solutions. For that purpose, **c4b**[shh] and **c4b**[ahh] were generated from a solution of the disulfide **4b** by irradiation with λ_{ex} = 365 nm, as described

above, prior to the addition of DNA. The absorption of ligand **2b** and **4b** decreased upon addition of DNA, and new red-shifted absorption maxima developed at 418 nm ($\Delta\lambda_{abs}$ = 14 nm, **2b**) and 423 nm ($\Delta\lambda_{abs}$ = 16 nm, **4b**) (Fig. 4). Only during the DNA titration of **2b**, an isosbestic point at 413 nm was formed, which indicated only one major binding mode. In the case of **4b**, however, the absorbance between 350–415 nm initially decreased, and the red-shifted maximum of **4b** only started to develop at a ligand–DNA ratio (LDR) of 5.7 as the result of at least two competing binding events. In contrast, the absorption spectra of **c4b**[shh] and **c4b**[ahh] or **6** did not or only marginally change upon addition of DNA, respectively (*cf.* ESI, Fig. S27†). Fitting of the binding isotherms from the photometric titration data to the non-competitive DNA-binding model[31] gave a binding constant of $K_b = 2.0 \times 10^4$ M^{-1} for **2b** (*cf.* ESI, chapter 5.4†). Unfortunately, a reasonable fit for the binding isotherm of **4b** could not be obtained from the titration data.

The fluorescence of the thioacetate **2b** was quenched with increasing DNA concentration whereas the fluorescence of **4b** firstly increased at the beginning of the titration and was quenched only at higher DNA concentrations (*cf.* ESI, Fig. S28†). The fluorescence of the benzo[*c*]thiophene **6** only increased marginally upon addition of DNA (*cf.* ESI, Fig. S28†). The data from the fluorimetric titration of **2b** were also used to determine a binding constant of $K_b = 2.0 \times 10^4$ M^{-1} for this ligand (*cf.* ESI, chapter 5.4†), which is in agreement with the one derived from the photometric titrations.

To obtain further information about the binding mode of **2b**, **4b**, **c4b**[shh], **c4b**[ahh], and **6** with DNA, circular dichroism (CD) and flow linear dichroism (LD) spectra were recorded at different LDR (Fig. 4B and C, *cf.* ESI, chapter 5.3†). In the long-wavelength absorption range of the ligands **2b** and **4b**, *i.e.* where DNA does not absorb, the CD spectra showed a positive and a negative induced CD (ICD) signal, which increased with increasing LDR (Fig. 4B). As the disulfide **4b** showed very pronounced ICD signals, a polarimetric DNA titration was also performed (Fig. 4B2, inset). In contrast to the photometric titration of **4b**, which did not reveal an isosbestic point, an isoelliptic point was observed at 375 nm in the polarimetric DNA titration. Obviously, only the ligand that is complexed in the major binding mode exhibits an ICD signal, whereas ligands in competing binding modes give only weak or no ICD bands. This lack of ICD activity is often related to backbone association.[32] Fitting of the binding isotherms to the theoretical model[31] gave a binding constant of $K_b = 6.1 \times 10^5$ M^{-1} (**4b**) (*cf.* ESI, chapter 5.4†). In contrast, the photocyclomers **c4b**[shh] and **c4b**[ahh] and the benzothiophene **6** showed no ICD signal in their long-wavelength absorption region (*cf.* ESI, Fig. S30†).

Upon addition of DNA the thioacetate **2b** gave a steadily increasing negative LD signal with increasing LDR in the absorption range of the ligand (Fig. 4C1). The LD spectra of the DNA-bound disulfide **4b** are more complex. More precisely, distinct negative LD bands developed in the long-wavelength absorption range; however, the relative intensities of the separ-
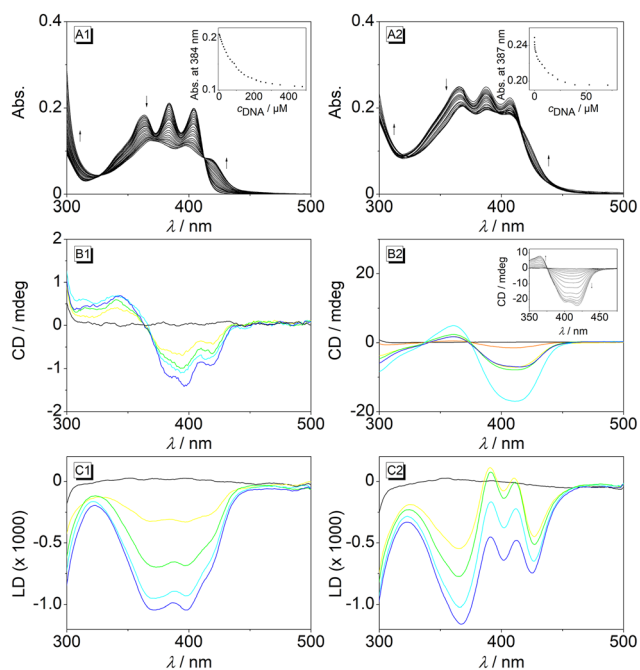

Fig. 4 Photometric (A, *c* = 20 μM), and polarimetric (CD: B, LD: C; c_{DNA} = 50 μM) titrations of **2b** (1) and **4b** (2) with ct DNA in bisphosphate EDTA (BPE) buffer (pH = 7.00); CD: LDR = 0 (black), 0.1 (orange), 0.5 (yellow), 1.0 (green), 1.5 (magenta), 2 (blue). The arrows indicate the change of the absorption bands during titration. Insets: A: plots of absorption *versus* DNA concentration; B: polarimetric DNA titration of **4b** (c_{DNA} = 100 μM) in BPE buffer (pH = 7.00).

This journal is © The Royal Society of Chemistry 2023

Org. Biomol. Chem., 2023, **21**, 5799–5808 | **5803**

ate maxima do not correlate with the ones observed during the photometric DNA titration of **4b** (Fig. 4C2), apparently indicating two overlapping LD bands with different phases. In agreement with the CD-spectra, both the photocyclomers **c4b**^shh and **c4b**^ahh and the benzo[*c*]thiophene **6** showed no pronounced LD signal in the long-wavelength absorption regions of the ligands (*cf.* ESI, Fig. S31†).

As the spectroscopic data of the complex between the disulfide **4b** and ct DNA pointed to a strong binding to DNA and a more complex binding mode, a fluorescent indicator displacement (FID) experiment with the known DNA intercalator thiazole orange (**TO**, $K_b = 3.2 \times 10^5$ M^{-1})[33] was performed.[34] Upon titration of the ligand to the **TO**-DNA complex, the fluorescence decreased with increasing ligand concentration, which indicated the displacement of **TO** from the DNA binding site (*cf.* ESI, Fig. S29†). Accordingly, the analysis of the titration gave a PD50 value at 0.72 μM, *i.e.* the concentration at which 50% of **TO** is displaced.

Altogether, the spectroscopic analysis of **2b** showed the characteristic features of DNA intercalators, namely a weak ICD and a negative LD signal in the absorption range of the ligand, both of which developed steadily with increasing LDR.[32,35] These observations are in agreement with the ones of the previously reported isomeric thioacetate **2a**,[14] however, the binding constant of **2b** is slightly higher. As both ligands exhibit the same ICD pattern the accommodation of the benzoquinolizinium unit within the intercalation site is essentially the same, most likely with the long molecular axis perpendicular to the long axis of the DNA base pairs.[16] Hence, the different binding constants reflect the different attractive or repulsive interactions of the substituent with the binding site, the grooves or the DNA backbone. In particular, the slightly higher affinity of isomer **2b** may originate from attractive binding interactions, *e.g.*, hydrogen bonding, of the thioester group with the nucleic bases pointing inside the grooves,[36] which is not the case with the isomer **2a**.

In contrast to the results with **2b**, the CD and LD spectra of the disulfide **4b** did not reveal one distinct binding mode with DNA. While the strong ICD signal points to the presence of a groove binder, the pattern of the LD signals indicates an overlap of bands resulting from different absorbing entities, and thus from different electronic transitions, related to the two separate benzoquinolizinium units in **4b**. By analogy, it is therefore proposed that the disulfide **4b** has a similar DNA binding mode as the isomer **4a**,[14] that is, it intercalates with one benzoquinolizinium unit into the DNA, resulting in a negative LD signal, whereas the other heteroaromatic unit is accommodated in the groove, which causes a positive LD band.[32] In this particular binding mode the ligand occupies several neighboring binding sides, which explains the irregular trend during the photometric titration which prevented the determination of a reasonable binding constant. Specifically, at the beginning of the titration, *i.e.* when DNA is added to the ligand, the large excess of ligand and paucity of available binding sites do not allow to form the preferred binding mode under these conditions. In contrast, in the polarimetric titra-

tions the ligand **4b** was titrated to the DNA, so that high ligand loading was avoided.

In agreement with the higher binding affinity of **4b** the PD50 value of the ligand was smaller than that of **4a**, that is, it displaces **TO** already at lower concentrations.[14] Furthermore, the difference of the DNA binding affinities of the isomers **4a** and **4b** follows the same trend as the one of the isomeric thioacetates **2a** and **2b**, because in both cases the affinity of the ligand with the substituent at position 7 of the benzoquinolizinium units is about twice as high as that of the 9-substituted isomer. This observation indicates that the accommodation of benzoquinolizinium derivatives with a thiomethylene-substituent in position 7 is energetically slightly more favored, presumably because of a better fit in the respective binding sites.

In analogy to the results with the photocyclomers of disulfide **5a** the spectra of the photocyclomers **c4b**^shh and **c4b**^ahh in the presence of DNA point to a very weak interaction with DNA, which may be explained by insignificant unspecific ionic interactions and a weak association with the DNA backbone.[14,32] In the case of compound **6**, the polarimetric titrations of **6** indicate that the ligand does not interact at all with DNA. In comparison with the thioacetate **2b** and the disulfide **4b**, the π-system of **6** is smaller, and it does not have a permanent positive charge, either, so that the required features of an efficient DNA intercalator are missing. Notably, there are a few reports about DNA-binding thiophene derivatives,[37] however, in these cases, the benzothiophene is part of a larger π-system, or contains additional heteroatoms. Moreover, there is one example of a thiophene-based topoisomerase II inhibitor that does not interact with DNA by intercalation.[38]

Enzymatic and reductive formation of 6 in the presence of DNA

As the thioacetate **2b** and the photocyclomers **c4b**^shh and **c4b**^ahh can be converted to the respective benzo[*c*]thiophene derivative **6** through the corresponding intermediate thiol **3b**, it was further investigated whether (a) the enzymatic release of **6** from **2b** can be performed in the presence of DNA and (b) whether **6** can be derived from the disulfide **4b** by a photocycloaddition–reduction-sequence in the presence of DNA (Fig. 5). In particular, these approaches should be applied as
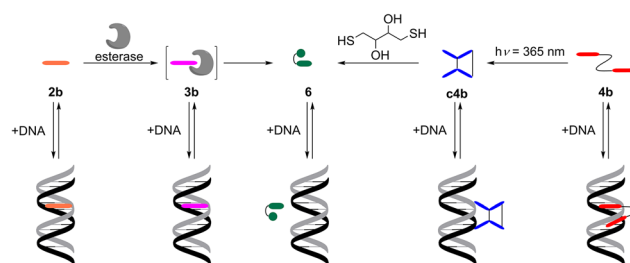

Fig. 5 Illustration of the *in situ* deactivation of DNA ligands **2b** and **4b** by enzymatic reduction of the thioacetate **2b** and by a photocycloaddition–reduction-sequence of the disulfide **4b** in the presence of DNA.

5804 | *Org. Biomol. Chem.*, 2023, **21**, 5799–5808

This journal is © The Royal Society of Chemistry 2023

complementary variations of the deactivation–reactivation concept,[14] specifically as controlled shut-off of the DNA association of the ligands **2b** and **4b** by the formation of the intermediate **3b** to product **6**.

When the thioacetate **2b** was incubated with the esterase in the presence of DNA the initial absorption of the benzoquinolizinium vanished and absorption bands of **6** evolved after 18 h, however, the absorption bands of the unknown side product were also observed (Fig. 6A1). Furthermore, the ICD signal of the thioacetate **2b** decreased and a less pronounced ICD signal developed over time in the range of 370–440 nm (Fig. 6B1).

Upon irradiation of the DNA-bound disulfide **4b** the absorption of the ligand steadily decreased and its characteristic ICD signal vanished. At the same time, no new ICD bands were observed, which is consistent with the formation of photoproducts **c4b^shh** and **c4b^ahh** in the presence of DNA (Fig. 6A2 and B2). Subsequently, DTT was added to the photocyclomer and the absorbance increased over the course of 1 h with formation of the characteristic absorption and CD bands of a benzoquinolizinium at 340–440 nm. Over the course of 16 h the absorption and CD bands steadily decreased and a new absorption band with maxima at 320–370 nm evolved. The CD spectrum after the enzymatic reduction matched the one obtained after reduction with DTT, but the absorbance at 370–440 nm was higher in the latter case. As the thiophene **6** showed no ICD bands in the presence of DNA, these signals likely correspond to the above-mentioned byproduct of the conversion of **3b**.

These experiments demonstrated that the DNA-binding ligands **2b** and **4b** can be deactivated *in situ* by the formation of the benzo[c]derivative **6** either with the enzymatic ester cleavage of **2b** or with a photocycloaddition–reduction-sequence of the disulfide **4b**. Most notably, in this photocycloaddition–reduction-sequence four different DNA binding modes can be generated starting from **4b**. The photometric and polarimetric analysis of theses sequences confirms the formation of **3b** as a reactive intermediate by its characteristic absorption and ICD bands. In particular, the bisignate ICD signal is consistent with intercalation of this intermediate as DNA binding mode.[14,35] Therefore, it is deduced from these data that the intermediate thiol **3b** intercalates into DNA like its isomer **3a**.[14]

Conclusions

In summary, a complementary example of a disulfide-functionalized photochromic system is presented that enables the control of DNA-binding properties by a combination of a photocycloaddition reaction and the redox reactions of the sulfide/disulfide functionalities. As compared with the photochemical and chemical reactivity of the isomeric disulfide **4a** and its photoproducts, it is shown that even a simple structural change, *i.e.* change of linker position, leads to significantly different – even unexpected – properties in the case of the **4b**. In particular, the strong DNA binder **4b** can be deactivated by irradiation as well as by chemically induced reduction. Likewise, by reaction with sulfides the photoproducts **c4b^shh** and **c4b^ahh**, that do not bind to DNA, can also be transformed to an intermediate intercalator **3b**, which in turn is deactivated by chemical reaction to the final product **6**. In general, this sequence provides general principles for the development of tools to establish and shut-off DNA-binding events by different orthogonal stimuli. It may be of special interest for future biological applications that the reactivity of the disulfide unit may respond differently to the specific oxidative and reductive environment in different cell types, especially considering the hypoxic nature of some cancer cells. Thus, it may be proposed that the DNA-related bioactivity of compounds with these particular features is not only controlled by external irradiation but may also be triggered by internal stimuli within the actual cell environment. Therefore, the investigation of these processes in cells, specifically the different impact on cytotoxicity in normoxic and hypoxic cells, will be the main focus of future studies.
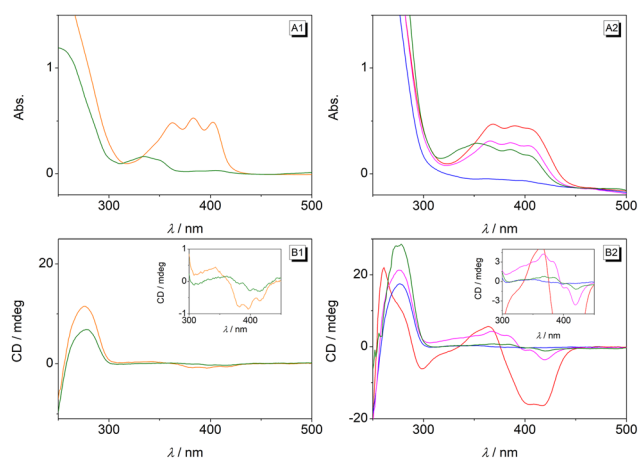

Fig. 6 Absorption (A) and CD spectra (B) of **2b** (c = 50 μM, 1) with ct DNA (c = 50 μM) in the absence (orange) and in the presence of esterase (400 μg, 7.6 units, T = 37 °C, t = 18 h) (green) and **4b** (c = 75 μM, 2) with ct DNA (c = 150 μM) before (red) and after irradiation (λ_{ex} = 365 nm, t = 4 min, blue) and subsequent treatment with DDT (c = 2 mM, T = 37 °C, t = 1 h, purple; t = 16 h, olive) in phosphate buffer solution (pH = 7.8).

Experimental section

Equipment

NMR spectra were recorded on a Jeol JNM-ECZR ([1]H: 500 MHz, [13]C: 125 MHz) or on a Varian VNMR-S 600 ([1]H: 600 MHz, [13]C: 150 MHz). The chemical shifts (δ) are given in ppm and are referenced relative to the sodium salt of trimethylsilylpropionic acid (TMSP-d_4, [1]H: δ = 0 ppm, [13]C: δ = 0 ppm) or the respective residual solvent signals (DMSO-d_5, [1]H: δ = 2.50 ppm, [13]C: δ = 39.5 ppm). In general, the HH coupling is specified as [1]J, [2]J, *etc*. When the unambiguous assignment was not possible, this information was omitted. Spectra were pro-

cessed with the software MestReNova 12.0.0. High-resolution (ESI) mass spectra were acquired with a Thermo Fisher Scientific Exactive MS with Orbitrap mass analyzer (injection flow rate: 10 µL min^{-1}, ESI spray voltage: 4.0 kV). Elemental analyses were determined in-house with a HEKAtech EUROEA combustion analyser (Universität Siegen, Organische Chemie I) or directly from the manufacturer HEKAtech GmbH-Analysenservice. Irradiation experiments were performed with a LED lamp (Roschwege HighPower-LED UV, λ_{exc} = 365 nm). Irradiation experiments monitored by NMR spectroscopy were performed in Boro400-5-7 tubes.

Reagents and solvents

Commercially available chemicals were used without further purification unless stated otherwise. Chemicals were purchased from the following companies: Acros Organics (Geel, BE): Br_2, pyridine-2-carbaldehyde, thioacetic acid. Carbolution (St Ingberd, DE): 1,4-dithio-DL-threit. Fluorochem (Graphite Way, EN): hydrobromic acid (aq. 48%). Carl Roth GmbH & Co KG (Karlsruhe, DE): L-glutathion. 7-(Bromomethyl)benzo[b]quinolizinium bromide (5)[21] was synthesized by reaction of 1,2-bis(1-methylene-2-[1,3-dioxolan-2-yl]pyridinium)phenyl bromide[39] with aqueous hydrobromic acid (48%).[21]

Buffer solutions were prepared in deionized water. The pH values were adjusted with aqueous solutions of NaOH or HCl. Prior to use, the buffer solutions were filtered through a PVDF membrane filter (pore size 0.45 µm).

BPE buffer: Na_2HPO_4 (6.00 mM), NaH_2PO_4 (2.00 mM), Na_2EDTA (1.00 mM).

PBS buffer: NaCl (137 mM), KCl (2.68 mM), KH_2PO_4 (1.98 mM), Na_2HPO_4 (10.0 mM).

Synthesis

7-([Acetylthio]methyl)benzo[b]chinolizinium bromide (2b). To a stirred suspension of **5** (590 mg, 1.67 mmol) in anhydrous DMF (20 mL) was added thioacetic acid (200 µL, 185 mg, 2.43 mmol) under argon-gas atmosphere and the suspension was stirred at 140 °C until all solids dissolved. After cooling to room temperature the solution was stirred for 3 d at r.t. The reaction mixture was added dropwise into a solution of EtOAc (300 mL) under vigorous stirring. The resulting precipitate was filtered off, washed with EtOAc (3 × 50 mL) and Et$_2$O (1 × 50 mL), and recrystallized from MeCN to give the product as yellow needles (483 mg, 83%); mp 172 °C (dec.). ^{1}H-NMR (500 MHz, DMSO-d_6): δ = 2.40 (s, 3H, CH$_3$), 4.79 (s, 2H, CH$_2$), 7.99–8.06 (m, 3H, 3-H, 8-H, 9-H), 8.13 (ddd, ^3J = 9 Hz, ^3J = 7 Hz, ^4J = 1 Hz, 1H, 2-H), 8.31 (d, ^3J = 9 Hz, 1H, 10-H), 8.58 (d, ^3J = 9 Hz, 1H, 1-H), 9.27 (s, 1H, 11-H), 9.39 (d, ^3J = 6.8 Hz, 1H, 4-H), 10.60 (s, 1H, 6-H). ^{13}C-NMR (125 MHz, DMSO-d_6): δ = 29.9 (CH$_2$), 30.9 (CH$_3$), 123.2 (C3), 125.0 (C6a), 126.0 (C11), 127.3 (C1), 127.4 (C10), 131.9 (C8), 132.1 (C2), 134.7 (C9), 135.0 (C4), 136.0 (C7), 136.5 (C10a), 137.9 (C6 or C11a), 138.0 (C6 or C11a), 195.2 (CO). MS (ESI$^+$): m/z (%) = 268 (100) [M − Br$^-$]$^+$. El. Anal. for C$_{16}$H$_{14}$BrNOS, calcd (%): C 55.18, H 4.05, N 4.02, S 9.21, found (%): C 55.24, H 3.83, N 4.26, S 9.59.

7-(Sulfanylmethyl)benzo[b]chinolizinium bromide (3b). A solution of **2b** (100 mg, 287 µmol) in aq. HBr (48%, 4 mL) was stirred for 5 h at 80 °C under argon-gas atmosphere. After cooling to r.t. the solution was cooled to −30 °C until a precipitate had formed. The yellow solid was suspended in THF (40 mL), filtered, and washed with Et$_2$O (2 × 20 mL) to give a yellow solid, (79 mg, 90%), 178 °C (dec). ^{1}H-NMR (500 MHz, DMSO-d_6): δ = 3.55 (t, ^3J = 8 Hz, 1H, SH), 4.44 (d, ^3J = 8 Hz, 2H, CH$_2$), 7.98 (dd, ^3J = 7 Hz, 1 Hz, 1H, Ar–H), 8.01 (td, ^3J = 7 Hz, ^4J = 2 Hz, 1H, Ar–H), 8.05 (dd, ^3J = 9 Hz, ^3J = 7 Hz, 1H, Ar–H), 8.11 (ddd, ^3J = 9 Hz, ^3J = 7 Hz, ^4J = 1 Hz, 1H, Ar–H), 8.28 (d, ^3J = 8 Hz, 1H, Ar–H), 8.57 (d, ^3J = 8 Hz, 1H, Ar–H), 9.26 (s, 1H, 11-H), 9.46 (d, ^3J = 7 Hz, 1H, 4-H), 10.70 (s, 1H, 6-H).

7,7′-(Disulfanediylbis[methylene])bis-benzo[b]quinolizinium bromide (4b). A solution of **2b** (250 mg, 718 µmol) in aq. HBr (48%, 2 mL) was stirred for 6 h at 100 °C. After cooling to room temperature, the solution was diluted with aq. acetic acid (96%, 3 mL), and Br$_2$ (70 µL, 0.22 g, 1.4 mmol) was added dropwise under vigorous stirring. The resulting suspension was stirred for 10 min at r.t. and poured into a solution of THF (200 mL). The precipitate was filtered off, washed with THF (3 × 50 mL) and Et$_2$O (1 × 10 mL), and crystallized from MeOH to furnish the product as an amorphous yellow solid (199 mg, 91%); mp 225 °C (dec.). ^{1}H-NMR (500 MHz, DMSO-d_6): δ = 4.62 (s, 2H, 2 × CH$_2$), 7.81 (dd, ^3J = 7 Hz, ^4J = 1 Hz, 1H, 8-H, 8′-H), 7.97–8.03 (m, 2H, 2-H, 2′-H, 9-H, 9′-H), 8.11 (dd, ^3J = 9 Hz, ^3J = 7 Hz, 1H, 3-H, 3′-H), 8.27 (d, ^3J = 9 Hz, 1H, 10-H, 10′-H), 8.57 (d, ^3J = 9 Hz, 1H, 4-H, 4′-H), 9.24 (s, 1H, 11-H, 11′-H), 9.39 (d, ^3J = 7 Hz, 1H, 1-H, 1′-H), 10.76 (s, 1H, 6-H, 6′-H). ^{13}C-NMR (125 MHz, DMSO-d_6): δ = 137.5 (C6, C6′), 137.4 (C11a, C11a′), 136.0 (C10a, C10a′), 134.8 (C7, C7′), 134.1 (C1, C1′), 133.8 (C9, C9′), 132.4 (C8, C8′), 131.5 (C3, C3′), 127.0 (C10, C10′), 126.8 (C4, C4′), 125.5 (C11, C11′), 124.2 (C6a, C6a′), 122.8 (C2, C2′), 36.9 (2 × CH$_2$). MS (ESI$^+$): m/z (%) = 225 (100) [M − 2Br$^-$]$^{2+}$. El. Anal. for C$_{28}$H$_{22}$Br$_2$N$_2$S$_2$·1.5 H$_2$O, calcd (%): C 52.76, H 3.95, N 4.39, S 10.06, found (%): C 53.01, H 3.95, N 4.50, S 10.04.

2-(Benzo[c]thiophen-4-ylmethyl)pyridine (6). A solution of **2b** (100 mg, 287 µmol) in aq. HBr (48%, 4 mL) was stirred for 5 h at 80 °C under argon-gas atmosphere. After cooling to r.t. the solution was cooled to −30 °C until a precipitate had formed. The yellow solid was suspended in THF (40 mL), filtered, and washed with Et$_2$O (2 × 20 mL) to give a yellow solid, which was redissolved in a solution of DMF (5 mL) and MeOH (20 mL). The solution was stirred for another 3 d at r.t. After removal of the solvents under reduced pressure, the brownish residue was submitted to flash column chromatography (SiO$_2$, neutral, CH$_2$Cl$_2$: MeOH, 95 : 5, R_f = 0.07, CH$_2$Cl$_2$: MeOH, 9 : 1) to give the product as a brownish oil (40 mg, 46%, calcd as hydrobromide). ^{1}H-NMR (500 MHz, DMSO-d_6): 4.40 (s, 2H, CH$_2$), 6.90 (dd, ^3J = 7 Hz, ^4J = 1 Hz, 1H, 5-H), 7.01 (dd, ^3J = 9 Hz, ^3J = 7 Hz, 1H, 6-H), 7.31 (dd, ^3J = 8 Hz, ^3J = 5 Hz, 1H, 5′-H), 7.40 (d, ^3J = 8 Hz, 1H, 3′-H), 7.54 (d, ^3J = 9 Hz, 1H, 7-H), 7.79 (td, ^3J = 8 Hz, ^4J = 2 Hz, 1H, 4′-H), 7.99 (d, ^4J = 3 Hz, 1H, 3-H), 8.00 (dd, ^4J = 3 Hz, ^4J = 1 Hz, 1H, 1-H), 8.46 (ddd, ^3J = 5 Hz, ^4J = 2 Hz, ^5J = 1 Hz, 1H, 6′-H). ^{13}C-NMR (125 MHz, DMSO-d_6): δ = 41.1 (CH$_2$), 116.3 (C1), 118.3 (C3), 120.7 (C7), 122.0 (C5′), 123.1

5806 | *Org. Biomol. Chem.*, 2023, **21**, 5799–5808

This journal is © The Royal Society of Chemistry 2023

(C5), 123.5 (C6), 123.7 (C3′), 131.8 (C4), 137.8 (C3a), 138.1 (C4′), 138.3 (C7a), 148.0 (C6′), 159.1 (C2′). HRMS (ESI$^+$): Calcd for: $[C_{14}H_{11}NS + H]^+$ m/z = 226.0685, found: 226.0681 $[M + H]^+$.

Conflicts of interest

There are no conflicts to declare.

Acknowledgements

References

1 (a) C. Chen, X. Li, H. Zhao, M. Liu, J. Du, J. Zhang, X. Yang, X. Hou and H. Fang, *J. Med. Chem.*, 2022, **65**, 3667; (b) G. Padroni, J. M. Withers, A. Taladriz-Sender, L. F. Reichenbach, J. A. Parkinson and G. A. Burley, *J. Am. Chem. Soc.*, 2019, **141**, 9555; (c) S. Bhaduri, N. Ranjan and D. P. Arya, *Beilstein J. Org. Chem.*, 2018, **14**, 1051.

2 W. Wu, Y. Pu and J. Shi, *J. Nanobiotechnol.*, 2022, **20**, 4.

3 (a) Q. Gao, J. Feng, W. Liu, C. Wen, Y. Wu, Q. Liao, L. Zou, X. Sui, T. Xie, J. Zhang and Y. Hu, *Adv. Drug Delivery Rev.*, 2022, **188**, 114445; (b) L. Conti, E. Macedi, C. Giorgi, B. Valtancoli and V. Fusi, *Coord. Chem. Rev.*, 2022, **469**, 214656.

4 J. K. Patra, G. Das, L. F. Fraceto, E. V. R. Campos, M. P. Del Rodriguez-Torres, L. S. Acosta-Torres, L. A. Diaz-Torres, R. Grillo, M. K. Swamy, S. Sharma, S. Habtemariam and H.-S. Shin, *J. Nanobiotechnol.*, 2018, **16**, 71.

5 X. Dong, R. K. Brahma, C. Fang and S. Q. Yao, *Chem. Sci.*, 2022, **13**, 4239.

6 H.-H. Han, H.-M. Wang, P. Jangili, M. Li, L. Wu, Y. Zang, A. C. Sedgwick, J. Li, X.-P. He, T. D. James and J. S. Kim, *Chem. Soc. Rev.*, 2023, **52**, 879.

7 (a) W. Xiao and J. Loscalzo, *Antioxid. Redox Signal.*, 2020, **32**, 1360; (b) J. J. Woods and J. J. Wilson, *Angew. Chem., Int. Ed.*, 2021, **60**, 1588.

8 (a) M. Zhou, Y. Xie, S. Xu, J. Xin, J. Wang, T. Han, R. Ting, J. Zhang and F. An, *Eur. J. Med. Chem.*, 2020, **195**, 112274; (b) J. Lin, D. Gao, S. Wang, G. Lv, X. Wang, C. Lu, Y. Peng and L. Qiu, *J. Am. Chem. Soc.*, 2022, **144**, 7667.

9 B. Sun, C. Luo, H. Yu, X. Zhang, Q. Chen, W. Yang, M. Wang, Q. Kan, H. Zhang, Y. Wang, Z. He and J. Sun, *Nano Lett.*, 2018, **18**, 3643.

10 R. Zhang, T. Nie, Y. Fang, H. Huang and J. Wu, *Biomacromolecules*, 2022, **23**, 1.

11 (a) Q. Laurent, R. Martinent, B. Lim, A.-T. Pham, T. Kato, J. López-Andarias, N. Sakai and S. Matile, *JACS Au*, 2021, **1**, 710; (b) Z. Shu, I. Tanaka, A. Ota, D. Fushihara, N. Abe, S. Kawaguchi, K. Nakamoto, F. Tomoike, S. Tada, Y. Ito, Y. Kimura and H. Abe, *Angew. Chem., Int. Ed.*, 2019, **58**, 6611.

12 (a) M. Lin, S. Zou, T. Li, J. Karges, Y. Chen, Y. Zhao, L. Ji and H. Chao, *Chem. Commun.*, 2022, **58**, 4324; (b) N. A. Simeth, S. Kobayashi, P. Kobauri, S. Crespi, W. Szymanski, K. Nakatani, C. Dohno and B. L. Feringa, *Chem. Sci.*, 2021, **12**, 9207; (c) M. Dudek, M. Deiana, K. Szkaradek, M. J. Janicki, Z. Pokładek, R. W. Góra and K. Matczyszyn, *J. Phys. Chem. Lett.*, 2021, **12**, 9436; (d) M. Deiana, M. Mosser, T. Le Bahers, E. Dumont, M. Dudek, S. Denis-Quanquin, N. Sabouri, C. Andraud, K. Matczyszyn, C. Monnereau and L. Guy, *Nanoscale*, 2021, **13**, 13795; (e) J. Rodriguez, J. Mosquera, S. Learte-Aymamí, M. Eugenio Vázquez and J. L. Mascareñas, *Acc. Chem. Res.*, 2020, **53**, 2286; (f) S. Kölsch, H. Ihmels, J. Mattay, N. Sewald and B. O. Patrick, *Beilstein J. Org. Chem.*, 2020, **16**, 111; (g) H. K. Saeed, S. Sreedharan and J. A. Thomas, *Chem. Commun.*, 2020, **56**, 1464; (h) D. V. Berdnikova, J. Heider, H. Ihmels, N. Sewald and P. M. Pithan, *ChemPhotoChem*, 2020, **4**, 520; (i) M. Linares, H. Sun, M. Biler, J. Andréasson and P. Norman, *Phys. Chem. Chem. Phys.*, 2019, **21**, 3637; (j) H. Chen, R. Li, S. Li, J. Andréasson and J. H. Choi, *J. Am. Chem. Soc.*, 2017, **139**, 1380; (k) T. C. S. Pace, V. Müller, S. Li, P. Lincoln and J. Andréasson, *Angew. Chem., Int. Ed.*, 2013, **52**, 4393; (l) M. Deiana, Z. Pokladek, K. Matczyszyn, P. Mlynarz, M. Bucklec and M. Samoca, *J. Mater. Chem. B*, 2017, **5**, 1028.

13 (a) J. Volarić, W. Szymanski, N. A. Simeth and B. L. Feringa, *Chem. Soc. Rev.*, 2021, **50**, 12377; (b) M. M. Lerch, M. J. Hansen, G. M. van Dam, W. Szymanski and B. L. Feringa, *Angew. Chem., Int. Ed.*, 2016, **55**, 10978.

14 C. Dohmen and H. Ihmels, *Org. Biomol. Chem.*, 2023, **21**, 1958.

15 (a) A. Granzhan and H. Ihmels, *Synlett*, 2016, **27**, 1775; (b) R. M. Suárez, P. Bosch, D. Sucunza, A. M. Cuadro, A. Domingo, F. Mendicuti and J. J. Vaquero, *Org. Biomol. Chem.*, 2015, **13**, 527; (c) S. Yamada, *Coord. Chem. Rev.*, 2020, **415**, 213601.

16 H. Ihmels, K. Faulhaber, D. Vedaldi, F. Dall'Acqua and G. Viola, *Photochem. Photobiol.*, 2005, **81**, 1107.

17 T. Wolff, C. Lehnberger and D. Scheller, *Heterocycles*, 1997, **45**, 2036.

18 A. Granzhan, H. Ihmels and M. Tian, *ARKIVOC*, 2015, 494.

19 S. A. Stratford, M. Arhangelskis, D.-K. Bučar and W. Jones, *CrystEngComm*, 2014, **16**, 10830.

20 H. D. Becker, *Chem. Rev.*, 1993, **93**, 145.

21 A. P. Krapcho and S. A. Cadamuro, *J. Heterocycl. Chem.*, 2004, **41**, 291.

22 R. P. Kreher and J. Kalischko, *Chem. Ber.*, 1991, **124**, 645.

23 C. K. Bradsher and J. P. Sherer, *J. Org. Chem.*, 1967, **32**, 733.

24 T. L. Wimmer, F. H. Day and C. K. Bradsher, *J. Org. Chem.*, 1975, **40**, 1198.

25 (a) M. A. O. Abdel-Fattah, A. H. Abadi, J. Lehmann, P. M. Schweikert and C. Enzensperger, *MedChemComm*,

This journal is © The Royal Society of Chemistry 2023

Org. Biomol. Chem., 2023, **21**, 5799–5808 | **5807**

2015, **6**, 1679; (*b*) M. D. Rozwadowska and A. Sulima, *Tetrahedron*, 2001, **57**, 3499.

26 (*a*) G. E. Gomez Pinheiro, H. Ihmels and C. Dohmen, *J. Org. Chem.*, 2019, **84**, 3011; (*b*) H.-J. Deiseroth, A. Granzhan, H. Ihmels, M. Schlosser and M. Tian, *Org. Lett.*, 2008, **10**, 757; (*c*) A. P. Krapcho, S. A. Cadamuro and L. Macnee, *ARKIVOC*, 2007, 28.

27 C. K. Bradsher and J. H. Jones, *J. Am. Chem. Soc.*, 1959, **81**, 1938.

28 H. Ihmels and J. Luo, *J. Photochem. Photobiol., A*, 2008, **200**, 3.

29 (*a*) C. Walling and R. Rabinowitz, *J. Am. Chem. Soc.*, 1959, **81**, 1243; (*b*) W. L. Wallace, R. P. van Duyne and F. D. Lewis, *J. Am. Chem. Soc.*, 1976, **98**, 5319; (*c*) M. You, Z. Zhu, H. Liu, B. Gulbakan Da Han, R. Wang, K. R. Williams and W. Tan, *ACS Appl. Mater. Interfaces*, 2010, **2**, 3601.

30 D. Gupta and A. R. Knight, *Can. J. Chem.*, 1980, **58**, 1350.

31 F. H. Stootman, D. M. Fisher, A. Rodger and J. R. Aldrich-Wright, *Analyst*, 2006, **131**, 1145.

32 T. Šmidlehner, I. Piantanida and G. Pescitelli, *Beilstein J. Org. Chem.*, 2018, **14**, 84.

33 J. Nygren, N. Svanvik and M. Kubista, *Biopolymers*, 1998, **46**, 39.

34 D. Monchaud, C. Allain and M.-P. Teulade-Fichou, *Bioorg. Med. Chem. Lett.*, 2006, **16**, 4842.

35 (*a*) B. Nordén, A. Rodger and T. Dafforn, *Linear Dichroism and Circular Dichroism. A Textbook on Polarized-Light Spectroscopy*, RSC Publishing, Cambridge, 2010; (*b*) N. C. Garbett, P. A. Ragazzon and J. B. Chaires, *Nat. Protoc.*, 2007, **2**, 3166.

36 V. Sharma, M. Gupta, P. Kumar and A. Sharma, *Curr. Pharm. Des.*, 2021, **27**, 15.

37 (*a*) K. Starcević, M. Kralj, I. Piantanida, L. Suman, K. Pavelić and G. Karminski-Zamola, *Eur. J. Med. Chem.*, 2006, **41**, 925; (*b*) M. Szymańska, M. Insińska-Rak, G. Dutkiewicz, G. N. Roviello, M. A. Fik-Jaskółka and V. Patroniak, *J. Mol. Liq.*, 2020, **319**, 114182; (*c*) W. Shi and T. L. Lowary, *Bioorg. Med. Chem.*, 2011, **19**, 1779.

38 K.-Y. Jun, H. Kwon, S.-E. Park, E. Lee, R. Karki, P. Thapa, J.-H. Lee, E.-S. Lee and Y. Kwon, *Eur. J. Med. Chem.*, 2014, **80**, 428.

39 C. K. Bradsher and J. C. Parham, *J. Org. Chem.*, 1964, **29**, 856.

5808 | *Org. Biomol. Chem.*, 2023, **21**, 5799–5808

This journal is © The Royal Society of Chemistry 2023